Temperature response of LOCTITE 648 anaerobic adhesive and hoop channels to enhance its effectiveness under high interference

TEMPERATURE RESPONSE OF LOCTITE 648 ANAEROBIC ADHESIVE AND HOOP CHANNELS TO ENHANCE ITS EFFECTIVENESS UNDER HIGH INTERFERENCE

D. Croccolo[a], M. De Agostinis[a], S. Fini[a], G. Olmi[a], L. Paiardini[a], F. Robusto[a]

[a] Department of industrial Engineering (DIN), University of Bologna, Viale del Risorgimento 2, 40136 Bologna, Italy

Corresponding Author:

Prof. Giorgio Olmi, Ph.D.

Department of Industrial Engineering (DIN)

University of Bologna

Viale del Risorgimento, 2 - 40136 BOLOGNA (BO) - ITALY

Phone: +39 051 2093455, +39 0543 374427 (in Forlì)

E - mail: giorgio.olmi@unibo.it

TEMPERATURE RESPONSE OF LOCTITE 648 ANAEROBIC ADHESIVE AND HOOP CHANNELS TO ENHANCE ITS EFFECTIVENESS UNDER HIGH INTERFERENCE

Abstract: The strength of a shaft-hub hybrid joint is affected by several factors, such as working temperature, interference level and coupling procedure. The first part of this study deals with temperature effect on the static response of shaft-hub hybrid joints. LOCTITE 648 anaerobic adhesive was applied for coupling 42CrMo4 tempered steel shafts to 16CrNi4Pb hardening steel hubs. The performance up to 100°C was experimentally investigated, involving press-fitted as well as shrink-fitted joints with interference up to 0.2%. Adhesive stripping upon coupling, adhesive degradation at high temperature and also frictional contribution decrease were highlighted. Afterwards, in the second part, the question of the adhesive being teared off under high interference was tackled. A hoop-channeled geometry was proposed, to increase the amount of adhesive remaining trapped at the joint interface. Hoop channels in the shafts proved to act as adhesive reservoir, thus facilitating adhesive dragging over the entire engagement length. Their effects on the joint strength were experimentally determined for both press-fitting and shrink-fitting coupling methods. The results, processed by the statistical tools of Analysis of Variance, orthogonality and pairwise tests, indicate the modified geometry is significantly beneficial for high interference press-fitted joints. Conversely, it may even be detrimental for shrink-fitted ones.

Keywords: Anaerobic Adhesive, Shaft-Hub, Shear Strength, Temperature, Adherent geometry, Press-Fit, Shrink-Fit.

List of Symbols:

A	Coupling surface for smooth shaft geometry [mm^2]
A_h	Coupling surface for hoop-channeled shaft geometry [mm^2]
d_c	Coupling diameter [mm]
E	Elastic modulus [MPa]
ξ	Specific Interference [-]
F_{ad}	Adhesive force [N]
F_{int}	Interference force [N]
F_{tot}	Decoupling force [N]
p_c	Coupling pressure [MPa]
Q_h	Hub constant [-]
$\tau_{Ad.}$	Adhesive static shear strength (averaged over the mating surface) [MPa]
μ_{ll}	First release friction coefficient [-]
$R_{a,h}$	Hub roughness [µm]
$R_{a,s}$	Shaft roughness [µm]
U_d	Nominal interference [mm]
Z_d	Real interference [mm]

List of Acronyms:

LSD	Least Significant Difference
PN	Press-fit without adhesive
PA	*Press fit with adhesive*
PA_100°C	*Press-fit with adhesive tested at 100°C*
PA_HC	*Press-fit with adhesive, shafts with hoop channels*
SN	*Shrink-fit without adhesive*
SA	*Shrink-fit with adhesive*
SA_100°C	*Shrink-fit with adhesive tested at 100°C*
SA_HC	*Shrink-fit with adhesive, shafts with hoop channels*

1. Introduction

The use of adhesives for joining mechanical components is widespread in many fields, such as automotive [1-3], aerospace [4-5], electrical [6-9]. Adhesives are used to connect parts of both the same material or different materials, to seal connections, to reduce the costs of conventional mechanical fasteners, to connect thin parts. They are also an ideal solution, when it is important to reduce weight, thanks to their high strength to weight ratio; moreover, sometimes they allow for an easier design of parts. Anaerobic adhesives are among the most suitable for connecting metal parts, for instance for the development of shaft-hub couplings. These may be arranged as hybrid joints, i.e. as interference-fitted and adhesively bonded couplings. A hybrid joint, if compared to a conventional interference-fitted one, makes it possible to carry higher torsional or axial loads even for lower interference levels. It also allows for lower tensile stresses acting on the hub at the coupling interface. Taking advantage of this point, material reduction can be put forward, which leads to lighter components. Moreover, when cyclic loads are present, the occurrence of fretting wear, which is frequent failure mode of interference-fitted joints under rotating bending, is also reduced, with a consequent beneficial outcome regarding fatigue life.

Hybrid joints design deals with two main resistance contributions: the first one, the interference term, is affected by contact pressure, contact area, materials properties, joint geometry and friction at the interface. The second one, namely, the contribution of the adhesive, depends on the adhesive shear strength and the coupling area. The first one can be affected by several factors, such as the operating temperature [10-14], humidity [15-17], the polymerization mode [18-19], the coupling pressure [20] and the coupling procedure [20-21].

Among the aforementioned parameters, the degradation as an effect of temperature is very important. For anaerobic adhesives, such as LOCTITE 648, the shear strength may be sharply decreased, as temperature is increased from 25°C to 100°C (LOCTITE 648

datasheet). It was observed [20] that the resistance contribution by the adhesive decreased significantly, as the level of interference increased; moreover, the mechanical response was also affected by the coupling method. That study was motivated by a real application concerning the coupling between a bevel gear and its shaft in an angular gearbox, taking advantage of both the geometrical interference and anaerobic adhesive. Angular gearboxes are likely to operate in environments, where temperatures may rise by many degrees due to heat dissipation. It must be remarked that specific studies dealing with the response of LOCTITE 648 under high temperature and involving practical applications in hybrid joints are missing in the literature. Therefore, with the aim of simulating the actual working conditions of an angular gearbox, push-out tests involving shaft-hub hybrid joints heated at 100°C were performed in the first part of the present study. In order to compare the results to those in [20], the specimens were coupled by both press-fitting and shrink-fitting, and the joint response under high temperature was subsequently assessed. Issues of novelty arise from considering the combined effects of both temperature and interference, involving joints coupled by different strategies, namely press-fitting as well as shrink-fitting.

A further outcome of the research in [20] is that the adhesive contribution decreases significantly, as the coupling interference increases, since the adhesive is stripped away upon coupling. Moreover, in press-fitted couplings (PF), high interference is likely to generate scratches, altering the mating surface. In addition, the rubbing during the assembly phase is often responsible for adhesive removal at the mating interface between the adherents. Even for shrink-fitted shaft-hub couplings (SF), the adhesive contribution may be dropped down by a high contact pressure.

In order to enhance the hybrid joint performance, a solution may be worked out to increase the amount of adhesive remaining trapped at the joint interface. An array of feasible approaches is discussed in the literature: a common strategy is increasing the

roughness of the adherent surfaces by a suitable treatment. The beneficial effect of a simple sanding treatment is discussed in [22-24], whereas the remarkably positive influence of a laser ablation treatment with a proper parameter setting is put forward in [25-27]. Joint mechanical performance enhancement is usually assessed in terms of increased static strength or of the failure mode being turned into cohesive. This last point is stressed in [28], where an extensive experimental campaign assisted by statistical tools made it possible to highlight the highly beneficial effect of sandblasting, especially, if run with the aid of a specific machine. Other studies, such as that in [29] have focused on a different approach, to enhance the strength of aluminum-to-aluminum bonded joints, making use of a suitable chemical etching, thus producing a beneficial surface alteration. Otherwise, hoop channels may be machined on the shaft, so that they can act as adhesive pockets. A similar approach was used in [5] in the development of a hybrid joint between a steel housing and a carbon-epoxy composite bush, making use of an anaerobic adhesive. In that study it was observed that, without hoop channels the adhesive became ineffective, as it was completely erased from the mating surface due to high interference. Machining hoop channels on the shaft makes it possible to create a portion of clearance needed for entrapping the adhesive. The hoop channels work as an adhesively bonded slip-fit joint, whereas the remaining portion of the joint acts as a conventional interference-fitted one [5].

Considering that no other applications are available in the literature, the possibility of exploiting properly machined hoop channels, to improve the adhesive effectiveness even under high interference, was here investigated. This was the subject of the second part of the present study, aimed at deriving tips for design under these conditions. In particular, the joint performance improvement, when steel shafts with hoop channels and smooth hubs are coupled under different interference levels, up to remarkably high ones, was studied. The coupling strategy was also investigated, accounting for both press-fitted and

shrink-fitted joints. Push-out tests were performed and statistical methods were applied, to compare the results to those of joints with smooth shaft geometry with and without adhesive.

2. Materials and Methods

The specimens were designed following the recommendations by Standard ISO 10123. However, proper adjustments were required, as this Standard deals with pin-and-collar joints, whereas interference was needed in the present study. The specimens were manufactured with 17 mm nominal coupling diameter and 13 mm coupling length, in order to have agreement with the geometry of the samples involved in the previous study [20]. Moreover, like in that campaign, to facilitate component handling, the shaft overall length was greater than that recommended by the Standard.

Material and treatment choice was steered by the angular gearbox application that motivated this study and that in [20], in order to have a good match between real components and samples. Shafts were made of 42CrMo4 tempered steel alloy, which exhibits good fatigue properties and is easy to supply. The hub material was 16CrNi4Pb hardened steel, which warrants a high hardness and wear resistance. Two geometries were used for the shafts: the first one with smooth cylindrical shape was used for high temperature tests (first part of the study). The second one, exhibiting two hoop channels in the coupling area, was used in the second part of the study, to assess the capability of this solution of overcoming the issue related to adhesive inefficiency under high inference. Sample geometries are shown in Fig. 1.

The hoop channels were designed with one millimeter width. The depth was chosen, so that the clearance with the hub was near to that recommended by the aforementioned Standard for pin-and-collar samples. Two channels were cut for each specimen. Due to

their presence, the coupling length available for interference was reduced to 11 mm, instead of 13 mm for the smooth geometry.

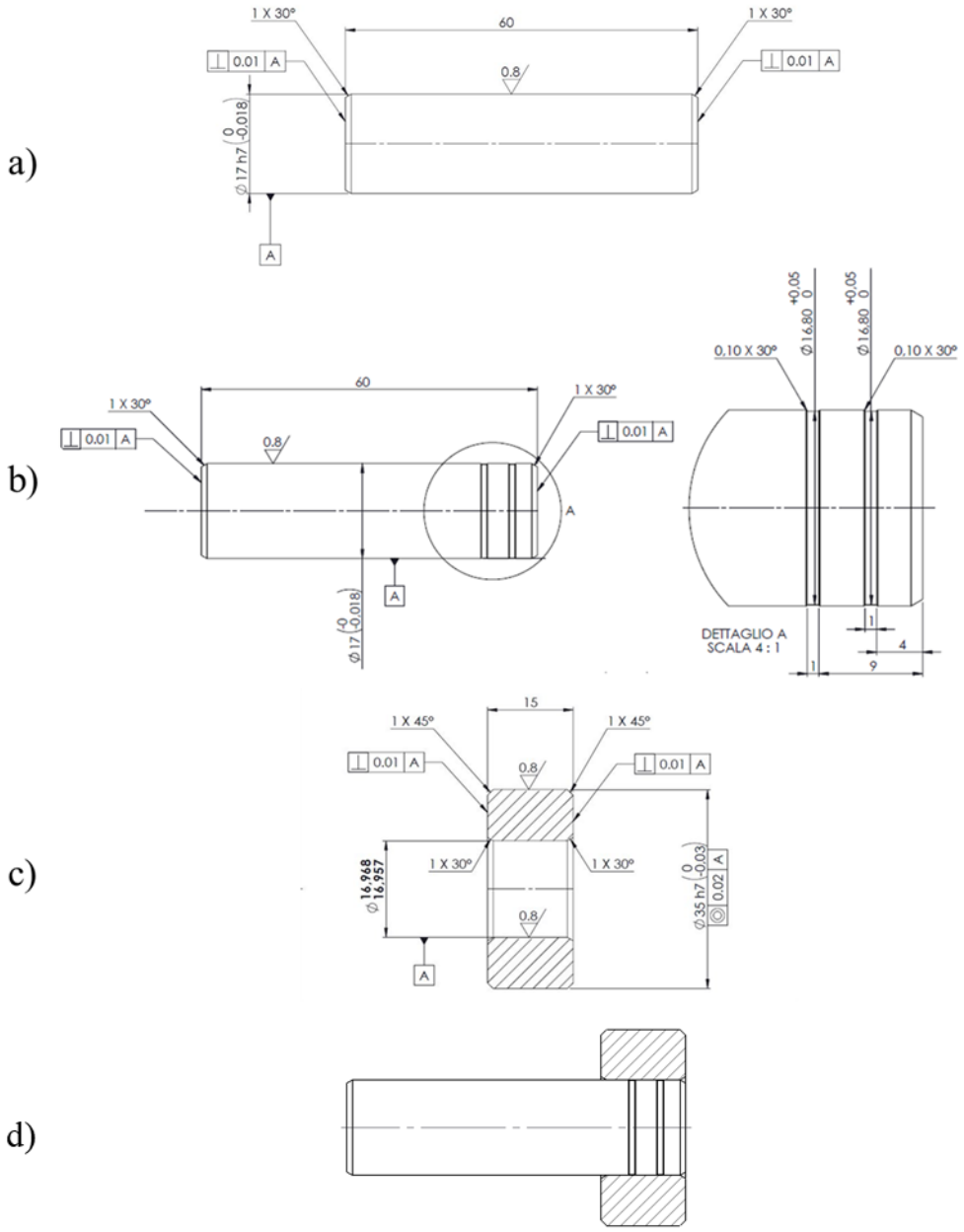

Figure 1: a) Smooth shaft geometry; b) shaft with hoop channels and its detail; c) hub geometry; d) shaft-hub assembly drawing with reference to a hoop-channeled shaft geometry (all dimensions are in mm)

All the dimensions involved in the coupling and in the expected joint performance were accurately checked. Shaft external diameters and hub internal diameters were measured by electronic micrometers with a certified accuracy of +/- 1 µm. The measurements were carried out in a metrology room at the temperature of 20 °C. The hoop channels

dimensions were checked by an electronic caliper for the diameter depth and a feeler gauge for the axial width. Furthermore, the eccentricity errors of the hubs, which could have altered the coupling pressure distribution, were verified by a cartesian measurement machine, as described in [20].

The real interference (Z_d), which differs in press-fitted couplings from the theoretical interference (U_d) was estimated by Eq. (1)

$$\boldsymbol{Z_d = U_d - 3 \cdot (R_{a_h} + R_{a_s})} \quad \textbf{(1)}$$

In this formula $R_{a,s}$ is the shaft roughness and $R_{a,h}$ the hub roughness, roughness values were determined along the axial direction by an electronic tester. As the retrieved values were very close for the shafts, the medium values (in particular, $R_{a,s}$ = 0.27 μm for smooth shafts and $R_{a,s}$ = 0.26 μm for those with hoop channels) were used for calculation purposes. As for the hubs, the actual measured values for each specimen were considered, when applying Eq. (1), due to higher scattering ($R_{a,h}$ medium value = 0.5 μm).

With reference to press-fitting coupling procedure, a hydraulic press (Instron 8032, equipped with a 100 kN load cell) was used to join the parts. As for shrink-fitted couplings, the hubs were heated in an oven (30 minutes at 250°C, based on the hub linear coefficient of thermal expansion, $12 \cdot 10^{-6}$ °C^{-1}) and the assembly was run manually, following the suggested procedure for pin-and-collars: the adhesive was applied by a little brush. All the samples, regardless of being planned for press-fitting or shrink-fitting, were preliminarily accurately polished by LOCTITE 7063. The adhesive involved in all the experimental campaigns was LOCTITE 648, which is a high strength, acrylic, anaerobic one. Its cure was carried out at 25°C for 72 hours, in order to achieve a nominal strength between 25 and 30MPa according to the adhesive datasheet.

The push-out tests under high temperature were performed at 100°C, as this level was regarded as realistic for the heating occurring during service of a gearbox. For this reason, further higher temperature levels have not been considered in the present study, as they

would have turned to be unfeasible in a real application. A heating chamber with forced convection was used to heat the coupled specimens up to 110°C. The heating temperature was deliberately set 10°C higher than the established one for testing, provided the specimens were expected to cool slightly during the test. The samples were extracted from the heating chamber one at a time and immediately tested, to prevent temperature drop: regarding this point, the PTFE insulation of the grips [20] helped to preserve heat. The shafts temperature was also checked by a thermocouple acting on the surface, which ensured temperature was always kept between 100°C and 105°C during every push-out trial. This must be regarded as a very small temperature variation: based on Loctite datasheet, just a 5°C variation at that temperature level is likely to induce a negligible variation of the adhesive strength. Therefore, this occurrence is not expected to affect result comparability.

All the push-out tests (under high temperature and at room temperature, with regard to specimens with hoop channels) were run in displacement-controlled conditions at the speed of 0.025 mm/s, in agreement with ISO 10123. However, in order to reduce the time of the experiment, the speed was incremented up to 1 mm/s after joint failure, corresponding to the force peak. The sampling rate was set at 30 Hz.

To determine the adhesive shear strength and to separate the adhesive and the interference contributions to the total release force, the principle of the superposition of the effects was used. The previous scientific literature is supportive for the application of this simple approach, provided that a strong (high strength) adhesive is involved. An experimental study [30] has involved hybrid joints operating under a different coupling pressure and subjected to a torque load. Their results indicate the joint strength increases linearly with the coupling pressure (to be regarded as the interference- or friction-related term) with the addition of a constant term depending on the shear strength by the adhesive (adhesive-related term). This outcome has been the subject of subsequent investigations and

analyses and a micromechanical model has been introduced in [31] to clarify the results. The developed model ensures the principle of the superposition of the effects keeps validity for a strong adhesive (like LOCTITE 648). Upon coupling, the adhesive is stripped away from the mating roughness crests, while it fills the voids in the valleys all around them, so that the joint resistance relies, on one hand, on the contact between adherent materials and, on the other hand, on the adhesive support.

The axial release force measured during the tests F_{tot} (Eq. (2)), namely the peak force, is yielded by the sum of the interference force F_{int} (Eq. (3)) and the adhesive force F_{ad} (Eq. (4)):

$$\boldsymbol{F_{tot} = F_{int} + F_{ad}} \quad \textbf{(2)}$$

$$\boldsymbol{F_{int} = \mu_{ll} \cdot p_c \cdot A} \quad \textbf{(3)}$$

$$\boldsymbol{F_{ad} = \tau_{ad} \cdot A} \quad \textbf{(4)}$$

Where μ_{ll} is the first release friction coefficient, p_c is the coupling pressure, A the mating area, and τ_{ad} the adhesive shear strength.

Eq. (3) keeps validity for samples with smooth shaft geometry, for which the mating area A consists in the entire cylindrical surface of the coupling. Conversely, for specimens with hoop-channeled shafts, the following (Eq. (5)) must be applied instead. In this case, the actual mating surface, regarded as A_h, is given by A, detracted by the surface corresponding to the hoop channels that is not available for interference fitting. It is worth mentioning that, even when hoop channels are present, the adhesive is expected to spread over the entire engagement length: therefore, Eq. (4) remains valid for both geometries. This point will also be discussed below.

$$\boldsymbol{F_{int} = \mu_{ll} \cdot p_c \cdot A_h} \quad \textbf{(5)}$$

From the quantitative point of view, A=694mm^2, arising from 17mm coupling diameter and 13mm engagement length. For the hoop-channeled geometry, A_h is 587mm^2, corresponding to the same coupling diameter and to an actual engagement length of

11mm (13mm, detracted by the total width of the two hoop channels). It must pointed out that the available area for frictional contact is therefore decreased by 15%, as an effect of hoop channels cutting.

For the coupling pressure p_c, the Lame's theory was applied, and, in case of shafts and hubs with the same elastic modulus, it corresponds to (Eq. (5)):

$$\boldsymbol{p_c = 0.5 \cdot \xi \cdot E \cdot (1 - Q_h^2)} \qquad \textbf{(6)}$$

Where E is the Young's modulus, Q_h is the aspect ratio defined as the ratio between the internal and the external diameters of the hub and is ξ the ratio between the real diametral interference Z_d (see Eq. (1)) and the nominal coupling diameter (d_c). All these relevant data are going to be provided below.

Experimental plan

In the first part of the study, dealing with shaft-hub joint temperature response, two factors (apart from temperature) were involved in the experimental plan: the specific interference and the coupling procedure. The specific interference ξ, namely the ratio between the real interference (Z_d) and the nominal coupling diameter (d_c), was set over four levels: $3 \cdot 10^{-4} \leq \xi \leq 5 \cdot 10^{-4}$, $9 \cdot 10^{-4} \leq \xi \leq 1.1 \cdot 10^{-3}$, $1.6 \cdot 10^{-3} \leq \xi \leq 1.8 \cdot 10^{-3}$ and $1.9 \cdot 10^{-3} \leq \xi \leq 2.1 \cdot 10^{-3}$. With regard to the coupling procedure, press-fitted (PF) and shrink-fitted (SF) joining techniques were considered. Five replications per level were also considered. The results retrieved in the push-out tests at room temperature (R.T.) [20] were included as well in the experiment for comparison purposes. The experimental design, where temperature is to be regarded as a third factor, is provided in Table 1. The release (peak) force and the subsequently determined adhesive shear strength were processed as output variables.

Table 1: Experimental plan regarding temperature effect, involving the three factors

Interference level	$3 \cdot 10^{-4} \leq \xi \leq 5 \cdot 10^{-4}$	Press-Fitted	Push-out tests at R.T.
			Push-out tests at 100°C
		Shrink-Fitted	Push-out tests at R.T.
			Push-out tests at 100°C
	$9 \cdot 10^{-4} \leq \xi \leq 1.1 \cdot 10^{-3}$	Press-Fitted	Push-out tests at R.T.
			Push-out tests at 100°C
		Shrink-Fitted	Push-out tests at R.T.
			Push-out tests at 100°C
	$1.6 \cdot 10^{-3} \leq \xi \leq 1.8 \cdot 10^{-3}$	Press-Fitted	Push-out tests at R.T.
			Push-out tests at 100°C
		Shrink-Fitted	Push-out tests at R.T.
			Push-out tests at 100°C
	$1.9 \cdot 10^{-3} \leq \xi \leq 2.1 \cdot 10^{-3}$	Press-Fitted	Push-out tests at R.T.
			Push-out tests at 100°C
		Shrink-Fitted	Push-out tests at R.T.
			Push-out tests at 100°C

In the second part of the research, further push-out tests were carried out, involving shafts with hoop channels and again accounting for different interference levels and both press-fitting and shrink-fitting coupling methods. The decoupling tests were carried out at room temperature, as it appears to be reasonable the mechanism involving adhesive shear strength degradation under high temperature is the same regardless of sample geometry. Moreover, the analysis was focused on the highest interference levels that are the most detrimentally affected by the occurrence of adhesive stripping. Therefore, three interference levels were considered instead of four: the two highest levels were kept barely unchanged with respect to those of the previous campaign. The third one can be

regarded as intermediate between the two previously considered lowest levels. The overall plan, including, for comparison purposes, the results for smooth shafts with and without the adhesive [20], is provided in Table 2.

The output variables and the tools used to process the data are the same as above.

Table 2: Experimental plan regarding hoop channel effect

Interference level			
Interference level	Low $6 \cdot 10^{-4} \leq \xi \leq 9 \cdot 10^{-4}$	Press-Fitted	Dry
			Adhesive smooth
			Adhesive Hoop channels
		Shrink-Fitted	Dry
			Adhesive smooth
			Adhesive Hoop channels
	Medium $1.5 \cdot 10^{-3} \leq \xi \leq 1.6 \cdot 10^{-3}$	Press-Fitted	Dry
			Adhesive smooth
			Adhesive Hoop channels
		Shrink-Fitted	Dry
			Adhesive smooth
			Adhesive Hoop channels
	High $2 \cdot 10^{-3} \leq \xi \leq 2.2 \cdot 10^{-3}$	Press-Fitted	Dry
			Adhesive smooth
			Adhesive Hoop channels
		Shrink-Fitted	Dry
			Adhesive smooth
			Adhesive Hoop channels

3. Results

The high temperature push-out test results are provided in Table 3 for press-fitted specimens and in Table 4 for shrink-fitted ones. The results are grouped by interference class. In the following tables, results involving push-out tests at room temperature using shafts with hoop channels are respectively shown for both press- (Table 5) and shrink-fitted (Table 6) coupling methods.

Table 3: Experimental results: push-out tests at 100°C for press-fitted specimens

Shaft ID	d_s *[mm]*	*Hub ID*	d_h *[mm]*	*Hub Roughness [μm]*	U_d *[mm]*	Z_d *[mm]*	*ξ[-]*	p_c *[MPa]*	*Decoupling Force* F_μ *[N]*
S1-01	16.996	H-161	16.960	0.310	0.036	0.034	0.0020	160	30,560
S1-03	16.996	H-165	16.960	0.929	0.036	0.032	0.0019	151	27,760
S1-04	16.996	H-177	16.960	0.555	0.036	0.034	0.0020	156	25,190
S1-15	16.996	H-188	16.960	0.444	0.036	0.034	0.0020	158	24,900
S1-19	16.996	H-199	16.960	0.423	0.036	0.034	0.0020	158	29,000
S1-68	16.994	H-170	16.964	0.629	0.030	0.027	0.0016	127	28,040
S1-76	16.994	H-200	16.964	0.464	0.030	0.028	0.0016	129	23,890
S1-77	16.994	H-214	16.964	0.336	0.030	0.028	0.0017	131	21,000
S1-02	16.993	H-33	16.963	0.562	0.030	0.028	0.0016	128	22,440
S1-26	16.993	H-43	16.963	0.643	0.030	0.027	0.0016	127	24,540
S1-149	16.986	H-40	16.968	0.448	0.018	0.016	0.0009	74	16,680
S1-157	16.986	H-64	16.968	0.420	0.018	0.016	0.0009	74	13,130
S1-161	16.986	H-80	16.968	0.417	0.018	0.016	0.0009	74	19,560
S1-85	16.985	H-01	16.967	0.505	0.018	0.016	0.0009	73	14,740
S1-90	16.985	H-19	16.967	0.478	0.018	0.016	0.0009	73	15,270
S1-96	16.983	H-78	16.975	0.563	0.008	0.006	0.0003	26	12,140
S1-97	16.983	H-18	16.974	0.427	0.009	0.007	0.0004	32	13,950
S1-100	16.983	H-21	16.974	0.505	0.009	0.007	0.0004	31	15,230
S1-110	16.983	H-47	16.974	0.515	0.009	0.007	0.0004	31	14,720
S1-128	16.983	H-72	16.974	0.532	0.009	0.007	0.0004	31	13,520

Table 4: Experimental results: push-out tests at 100°C for shrink-fitted specimens

Shaft ID	d_s *[mm]*	*Hub ID*	d_h *[mm]*	*Hub Roughness [μm]*	U_d *[mm]*	Z_d *[mm]*	*ξ[-]*	p_c *[MPa]*	*Decoupling Force* F_μ *[N]*
S1-09	16.998	H-79	16.962	0.682	0.036	0.036	0.0021	167	46,430
S1-16	16.998	H-99	16.962	0.518	0.036	0.036	0.0021	167	31,680
S1-27	16.998	H-100	16.962	0.656	0.036	0.036	0.0021	167	36,040
S1-28	16.998	H-103	16.962	0.505	0.036	0.036	0.0021	167	35,090
S1-34	16.998	H-109	16.962	0.443	0.036	0.036	0.0021	167	30,070
S1-33	16.995	H-08	16.965	0.341	0.030	0.030	0.0018	140	30,590
S1-37	16.995	H-10	16.965	0.476	0.030	0.030	0.0018	140	30,440
S1-38	16.995	H-44	16.965	0.434	0.030	0.030	0.0018	140	28,040
S1-44	16.995	H-48	16.965	0.639	0.030	0.030	0.0018	140	47,120
S1-48	16.995	H-52	16.965	0.746	0.030	0.030	0.0018	140	42,680
S1-82	16.987	H-23	16.970	0.335	0.017	0.017	0.0010	79	43,470
S1-89	16.987	H-29	16.970	0.421	0.017	0.017	0.0010	79	32,060
S1-93	16.987	H-09	16.969	0.262	0.018	0.018	0.0011	84	33,870
S1-105	16.987	H-11	16.969	0.522	0.018	0.018	0.0011	84	42,040
S1-113	16.987	H-34	16.969	0.481	0.018	0.018	0.0011	84	45,080
S1-108	16.984	H-55	16.979	0.501	0.005	0.005	0.0003	23	35,710
S1-114	16.984	H-61	16.979	0.413	0.005	0.005	0.0003	23	32,650

S1-120	16.984	H-65	16.979	0.731	0.005	0.005	0.0003	23	31,170
S1-121	16.984	H-69	16.978	0.697	0.006	0.006	0.0004	28	29,440
S1-125	16.984	H-215	16.978	0.544	0.006	0.006	0.0004	28	34,780

Table 5: Experimental results: push-out tests at room temperature. Press-fitted shafts with hoop channels

Shaft ID	*d_s [mm]*	*Hub ID*	*d_h [mm]*	*Hub Roughness [μm]*	*U_d [mm]*	*Z_d [mm]*	*ξ[-]*	*p_c [MPa]*	*Decoupling Force F_μ [N]*
S3-28	16.993	H-153	16.957	0.497	0.036	0.034	0.0020	157	39,050
S3-29	16.993	H-175	16.957	0.491	0.036	0.034	0.0020	157	43,690
S3-33	16.993	H-176	16.957	0.513	0.036	0.034	0.0020	156	44,530
S3-40	16.993	H-202	16.957	0.515	0.036	0.034	0.0020	156	43,970
S3-45	16.993	H-222	16.957	0.384	0.036	0.034	0.0020	158	39,290
S3-20	16.987	H-113	16.958	0.345	0.029	0.027	0.0016	126	36,880
S3-21	16.987	H-114	16.958	0.389	0.029	0.027	0.0016	126	40,540
S3-22	16.987	H-122	16.958	0.517	0.029	0.027	0.0016	124	41,390
S3-01	16.986	H-124	16.958	0.359	0.028	0.026	0.0015	121	38,360
S3-03	16.986	H-152	16.958	0.332	0.028	0.026	0.0015	122	39,150
S3-16	16.983	H-07	16.971	0.465	0.012	0.010	0.0006	46	23,820
S3-23	16.983	H-67	16.971	0.478	0.012	0.010	0.0006	45	20,650
S3-43	16.997	H-227	16.981	0.458	0.016	0.014	0.0008	64	29,460
S3-44	16.997	H-194	16.982	0.474	0.015	0.013	0.0008	59	27,920
S3-53	16.999	H-225	16.986	0.332	0.013	0.011	0.0007	52	22,280

Table 6: Experimental results: push-out tests at room temperature. Shrink-fitted shafts with hoop channels

Shaft ID	*d_s [mm]*	*Hub ID*	*d_h [mm]*	*Hub Roughness [μm]*	*U_d [mm]*	*Z_d [mm]*	*ξ[-]*	*p_c [MPa]*	*Decoupling Force F_μ [N]*
S3-27	16.994	H-164	16.956	0.587	0.038	0.038	0.0022	177	41,000
S3-36	16.994	H-182	16.956	0.612	0.038	0.038	0.0022	177	40,380
S3-46	16.994	H-02	16.957	0.402	0.037	0.037	0.0022	172	50,320
S3-51	16.994	H-107	16.957	0.630	0.037	0.037	0.0022	172	41,710
S3-54	16.994	H-112	16.957	0.709	0.037	0.037	0.0022	172	35,640
S3-06	16.987	H-04	16.962	0.367	0.025	0.025	0.0015	116	45,440
S3-09	16.987	H-139	16.962	0.467	0.025	0.025	0.0015	116	48,550
S3-11	16.987	H-156	16.962	0.605	0.025	0.025	0.0015	116	46,210
S3-17	16.987	H-115	16.962	0.641	0.025	0.025	0.0015	116	45,270
S3-18	16.987	H-119	16.962	0.414	0.025	0.025	0.0015	116	44,180
S3-10	16.985	H-17	16.971	0.605	0.014	0.014	0.0008	65	38,450
S3-12	16.985	H-68	16.969	0.370	0.016	0.016	0.0009	74	42,210
S3-14	16.985	H-42	16.970	0.497	0.015	0.015	0.0009	70	42,280
S3-19	16.985	H-50	16.970	0.541	0.015	0.015	0.0009	70	44,570
S3-26	16.985	H-51	16.970	0.498	0.015	0.015	0.0009	70	44,030

4. Discussion

4.1 High temperature tests.

The retrieved decoupling forces F_{tot} for the press-fitted samples are collected in the bar graph in Fig. 2 with variation intervals from minimum to maximum values. The "PA_100°C" set refers to high temperature push-out tests, whereas the "PA" bars deal with the decoupling tests at room temperature. All the results are grouped, based on the specific interference.

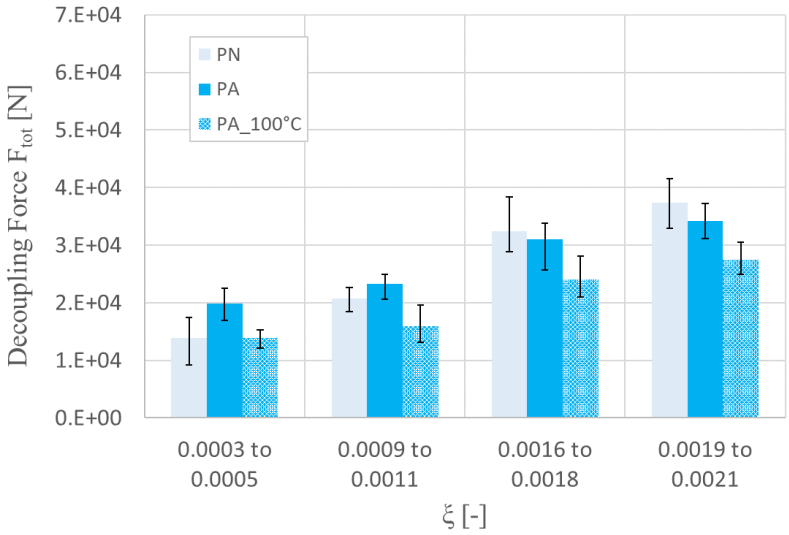

Figure 2: Decoupling force for press-fitted specimens. PN: dry coupled and decoupled at room temperature; PA: coupled with adhesive and decoupled at room temperature; PA_100°C coupled with adhesive and decoupled at 100°C.

The higher the interference level, the higher the push-out force, due to the effect of the higher contact pressure. Comparing the results to the decoupling force in dry condition (interference joint without adhesives, "PN" set), it is worth mentioning the adhesive provides a positive contribution only at the lowest levels of interference and only for room temperature working conditions. The effect of the interference level at room temperature has been widely investigated in previous studies [20]: when interference is high, the adhesive contribution is sharply dropped down to zero, as a large amount of adhesive is stripped away upon coupling. Regarding temperature, the release force drops down, when it rises. With respect to the room temperature condition, the mean force is reduced by

26% at 100°C. Increased temperature indeed leads to a deterioration of the adhesive performance, which is consistent to the strength drop involving other adhesive types such as epoxy adhesives [14]. In addition, it must be pointed out, the release force under high temperature is comparable to that in dry condition at lower interference, which is supportive for poor adhesive effect in this condition. However, a quite surprising outcome is that it becomes even lower at the other levels corresponding to greater interference.

It must be argued the temperature of the performed test is very close to the glass transition temperature, which is the threshold, beyond which the adhesive turns to have a rubber-like behavior [32]. As temperature reaches or exceeds this threshold, the molecular mobility increases and the mechanical properties consequently significantly change, involving, in particular, reduced stiffness and strength. For LOCTITE 648 the glass transition temperature is 100°C (based on LOCTITE 648 datasheet) and at this temperature the adhesive nominal shear strength drops down by 30% with respect to that at room temperature. This outcome clarifies well the worsening of the release force.

As highlighted above, an interesting point is temperature not only affects the adhesive performance, but also the interference-related contribution. This remark stems from the release force (with adhesive) under high temperature being lower than the release force in dry conditions at room temperature. This outcome is presumably due to friction coefficient decrease. This phenomenon has been investigated in the scientific literature, mainly in studies dealing with tribology and wear. As reported in [33], the friction coefficient drops down monothonically, as temperature increases, in particular in the range from 20 to 150°C. The experiment in this Ref. was conducted on a high strength steel, but similar results were found for a 0.45% C steel [34], which is a hardening steel with similar features to that used here for the shafts. Moreover, this phenomenon is studied and carefully considered in the field of brake design in automotive, as heat dissipation and temperature increase are likely to trigger pad friction coefficient drop and,

in turn, brake performance worsening. Therefore, the combined effect of the adhesive degradation and the reduction of the friction coefficient justifies, from the qualitative point of view, the occurrence detailed above. Some quantitative remarks will be given in the following.

The same comparisons for shrink-fitted samples are plotted in Fig. 3. When comparing decoupling results at room temperature (SA series) to those at 100°C (SA_100 series), a mean reduction by 28% affecting the decoupling force was observed.

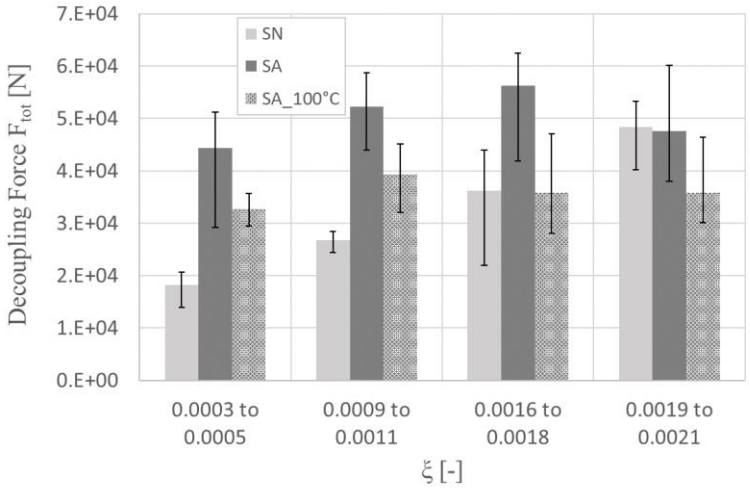

Figure 3: Decoupling force for shrink-fitted specimens. SN: dry coupled and decoupled at room temperature; SA: coupled with adhesive and decoupled at room temperature; SA_100°C: coupled with adhesive and decoupled at 100°C.

Unlike for press-fitted couplings, the adhesive contribution on the joint performance keeps significant even for higher interference levels under shrink-fitting [20]. However, the adhesive contribution vanishes at the highest interference level, as the amount of adhesive that remains trapped in the joint drops down due to the too small available clearance despite hub heating.

To statistically assess the effects of the adhesive contribution and of increased temperature on the release force, for both press-fitted and shrink-fitted couplings, an analysis of the variance was carried. The outcomes highlight a strong influence on the push-out force.

As a first remark, Fig. 2 and Fig. 3 indicate the release force is higher for shrink-fitted couplings than for press-fitted ones, regardless of the presence of the adhesive. The reason is that, under shrink-fitting, the crests of roughness do not flatten during assembly, thus contributing to an increased release force for the same level of nominal interference. Moreover, a larger amount of adhesive is retained, thanks to slight clearance upon coupling under temperature.

Combining the formulas in Eq. (2) and Eq. (4), it is possible to compute (Eq. (7)) the adhesive shear strength, thus isolating its contribution.

$$\boldsymbol{\tau_{ad} = \frac{F_{tot} - \mu_{ll} \cdot p_c \cdot A}{A}} \qquad (7)$$

F_{tot} was experimentally measured by the load cell, whereas p_c was calculated for each test, based on Eq. (6). The effect of temperature on the friction coefficient was accounted, reducing by 24% the values of μ_{ll} obtained in [20] at room temperature. These averagely range from 0.33 to 0.52 for press-fitted specimens and from 0.37 to 0.8 for shrink-fitted ones. Related comments are included in [20]. This reduction was applied, according to the aforementioned Ref.s [33-34] that deal with similar materials and with friction over the same temperature range (20 to 100 °C). The outcomes in terms of adhesive shear strengths are shown in Fig. 4 for press-fitted samples and Fig. 5 for shrink-fitted ones. Due to the temperature increment, the shear strength decrease is about 41% for press-fit at the lowest interference level and 28% for shrink-fit up to $\xi = 0.0011$. This drop is quite reasonable, as in the same order of that reported in the datasheet regarding the plain properties of the adhesive. Under higher interference levels, the percentage drop increases sharply. However, the data regarding shear strength at increased interference are not reliable: as highlighted above, they indicate most adhesive is teared off upon coupling due to the high contact pressure. At the highest interference level, the adhesive contribution drops down to zero.

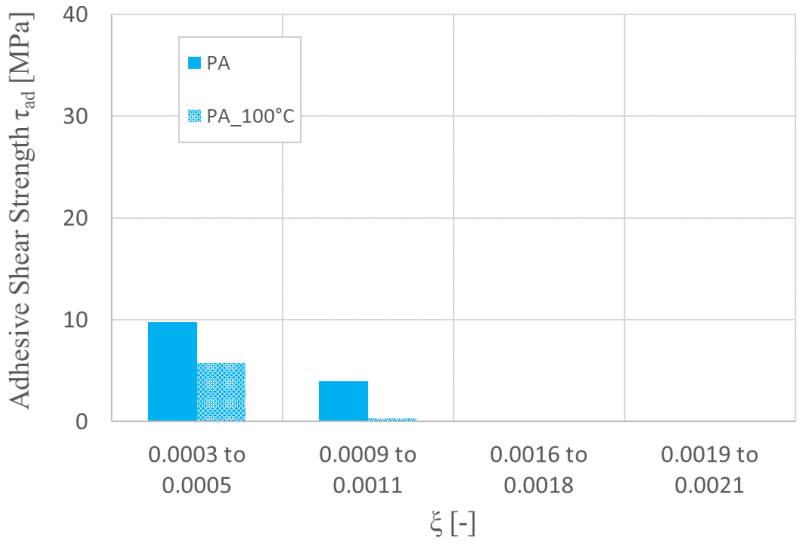

Figure 4: Adhesive shear strength (average values) for press-fitted samples tested at room temperature (PA) and at 100°C (PA_100°C)

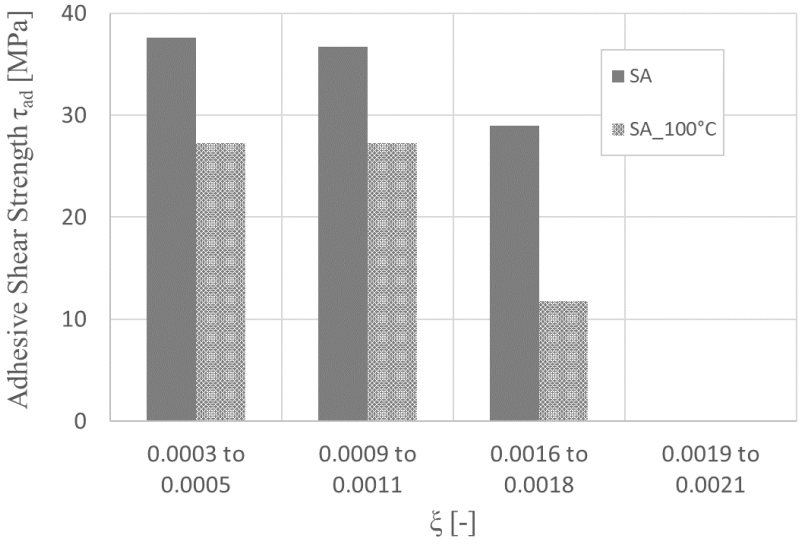

Figure 5: Adhesive shear strength (average values) for shrink-fitted samples tested at room temperature (SA) and at 100°C (SA_100°C)

4.2 Hoop channel cutting

As observed, under press-fitting, the decoupling force of the hybrid joint under huge interference is detrimentally affected by the adhesive being teared off upon coupling. A possible solution to overcome this issue is utilizing shrink-fitting, which leads to benefits in terms of joint performance. However, this coupling technique is more complicated and

expensive. A further option to overcome the described issue is changing the joint geometry. Therefore, a design with hoop channels (Fig. 1) was considered, trying to increase the amount of adhesive that remains trapped in the joint, thus improving the joint strength.

Regarding press-fitted and adhesively bonded samples, the decoupling forces obtained for specimens with hoop channels (PA_HC set) are compared to those for samples with smooth geometry (PA set) in Fig. 6. The results for smooth specimens without adhesive (dry) are appended as well (PN set).

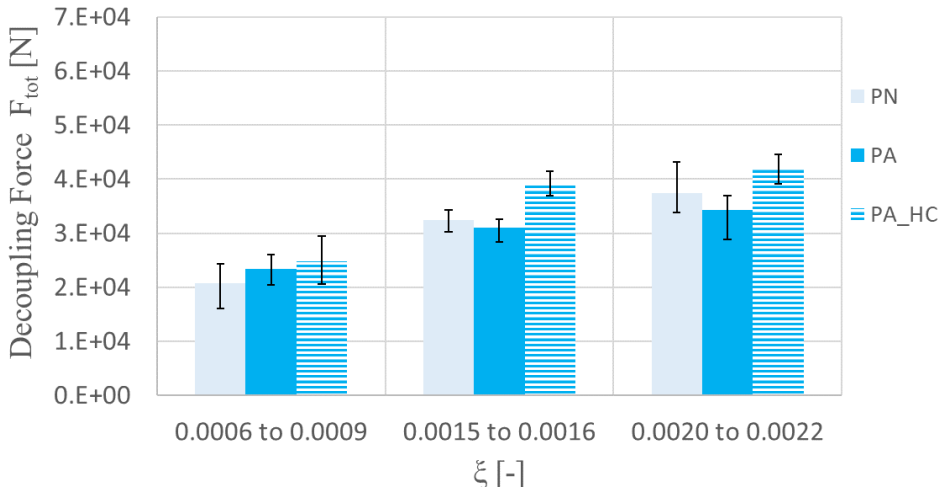

Figure 6: Decoupling force for press-fitted specimens. PN: dry coupled with smooth geometry; PA: coupled with adhesive with smooth geometry; PA_HC: coupled with adhesive with hoop channels.

The improved geometry leads to much higher decoupling forces. The results were also processed by the tool of analysis of variance that confirmed both the interference level and the geometry/coupling condition (dry vs. adhesive with smooth geometry vs. adhesive with hoop channels) significantly affect the joint release force. This analysis was subsequently deepened by allocation of the significant differences. The tools of pairwise tests and of variance orthogonal decomposition were used for this purpose. As for pairwise tests, the Fisher's Least Significance Difference (LSD) and the Newman’s Keuls tests were applied, to process the data retrieved at each interference level. The same data

were then processed by the tool of orthogonality, to isolate the amount of variance depending on the beneficial contribution of the hoop channels, to be compared to total variance. The outcomes of both the pairwise tests indicate that for medium and high interference levels the improvement yielded by the hoop channel geometry is highly significant with respect to the coupling with adhesive and smooth geometry. In turn, as above and in [20], the latter condition is well comparable to that without adhesive, as most of it gets erased.

These results are also confirmed by variance decomposition: for the top two interference levels, the largest amounts of variance are due to the different performance with and without hoop channels. The amounts of decoupling force variance arising from the different performance with and without adhesive and with and without hoop channels are collected in Fig. 7 (a) and (b) for high and medium interference levels respectively. Figure 7 (a), for instance, indicates decoupling force overall variance is 99% due the different resistance with and without hoop channels and just 1% due to the different response with and without adhesive.

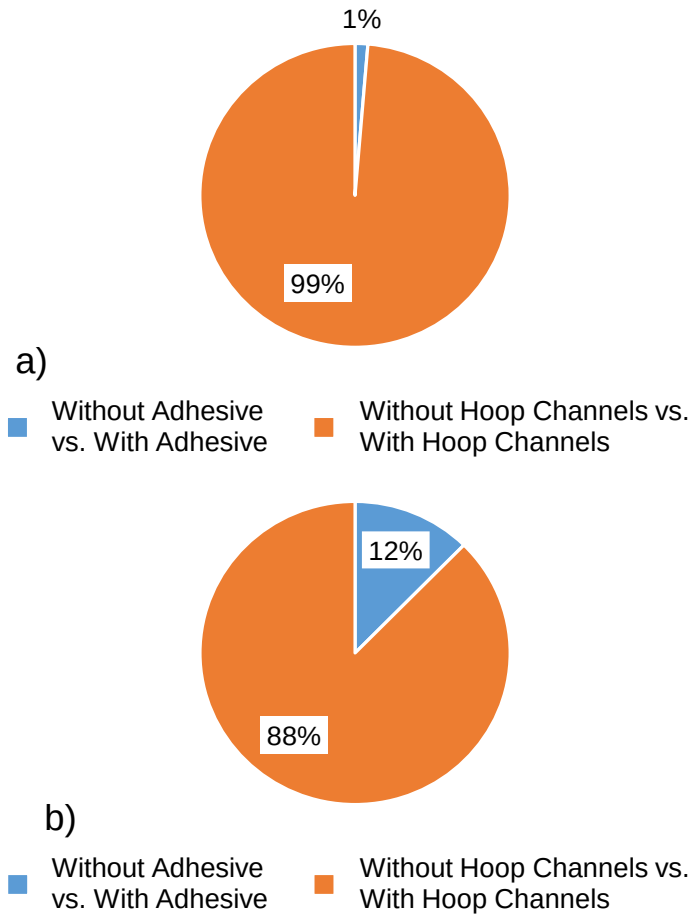

Figure 7: Orthogonal decomposition of the variance affecting the decoupling force (for press-fitting) under (a) high and (b) medium interference levels

Conversely, at lower interference level, the resistance increment provided by the hoop channels does not reach the significance threshold. This outcome means that for low interference a smooth geometry is still efficient at trapping a sufficient amount of adhesive. These outcomes may be qualitatively explained, observing that cutting hoop channels implies a decrease of the contact area (engagement length for friction) between the shaft and the hub, thus decreasing the interference contribution to the overall performance of the joint. However, this improved geometry compensates with a double positive effect. First, the hoop channels act as a supply reservoir for the adhesive: the hub, during its coupling with the shaft, drags the exceeding adhesive and spreads it slightly on the shaft, thus covering its entire coupling length. Secondly, the adhesive filling the hoop channels provides an additional contribution, being proportional to the adhesive shear

strength and to the area of the grooves, as for a slip-fit joint. From a quantitative point of view, at the top interference level, the interference-related term is averagely reduced from 31 to 27kN. It is worth mentioning this 15% drop is well aligned with the percentage drop of the available length for interference, following hoop channel machining. Moreover, this 15% decrement also corresponds to the same decrease of the available mating area in the channeled geometry. However, the adhesive contribution is highly magnified, considering it is negligible for the smooth geometry, for which interference only provides resistance against decoupling. Thus, the adhesive contribution is incremented from zero to around 27% of the overall decoupling force, taking advantage the channeled geometry. The same applies for the second top interference level, for which the adhesive contribution is again increased from negligible values to approximately 1/3 of the resistance against decoupling. The adhesive contribution enhancement clearly prevails on the interference force decrease.

The images in Fig. 8 show two press-fitted and adhesively bonded smooth shafts at medium (Fig. 8 (a)) and high (Fig. 8 (b)) interference. These are compared to press-fitted and adhesively bonded shafts with hoop channels for the same interference levels (Fig. 8 (c) and Fig. 8 (d)). It can be remarked the coupling surfaces in case of hoop-channeled geometry appear to be less scratched. In addition, areas with polymerized adhesive are slightly visible even far away from the hoop channels. Conversely, the surface of smooth shafts is badly damaged and no traces of adhesive can be observed.

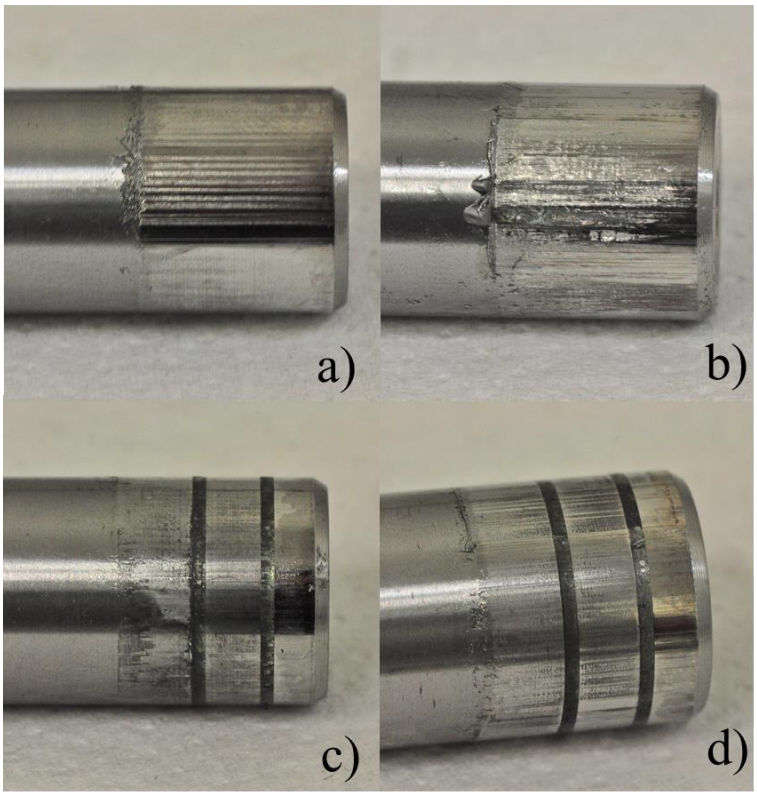

Figure 8: Press-fitted shafts. a) PA set, medium interference. b) PA set, high interference. c) PA_HC set, medium interference. d) PA_HC set, high interference.

The shear strength has been determined, according to the aforementioned model, based on the principle of the superposition of the effects (Eq.s (2, 4-5, 6)). Its value is yielded by Eq. (8) that replaces Eq. (7) for the channeled shaft geometry.

$$\tau_{ad} = \frac{F_{tot} - \mu_{ll} \cdot p_c \cdot A_h}{A} \quad (8)$$

This processing has led to the results collected in Fig. 9, where the beneficial contribution by the hoop channels is clearly visible. On one hand, for smooth shafts, the adhesive shear strength tends to zero at the two top levels of the specific interference range for this campaign, indicating the adhesive is completely teared off upon coupling, whereas a small amount is retained at the low level. On the other hand, when hoop channels are present, the shear strength reaches values between 15 and 20 MPa, even at the highest interference level. The retrieved values are a bit lower than the typical strength (which should be at least 25 MPa) for the investigated adhesive (according to its datasheet) but

confirm that, thanks to the hoop channels, the adhesive can work properly and provide a relevant contribution to the joint response. However, their collocation under the typical range may indicate that a small amount of adhesive is still stripped away during coupling.

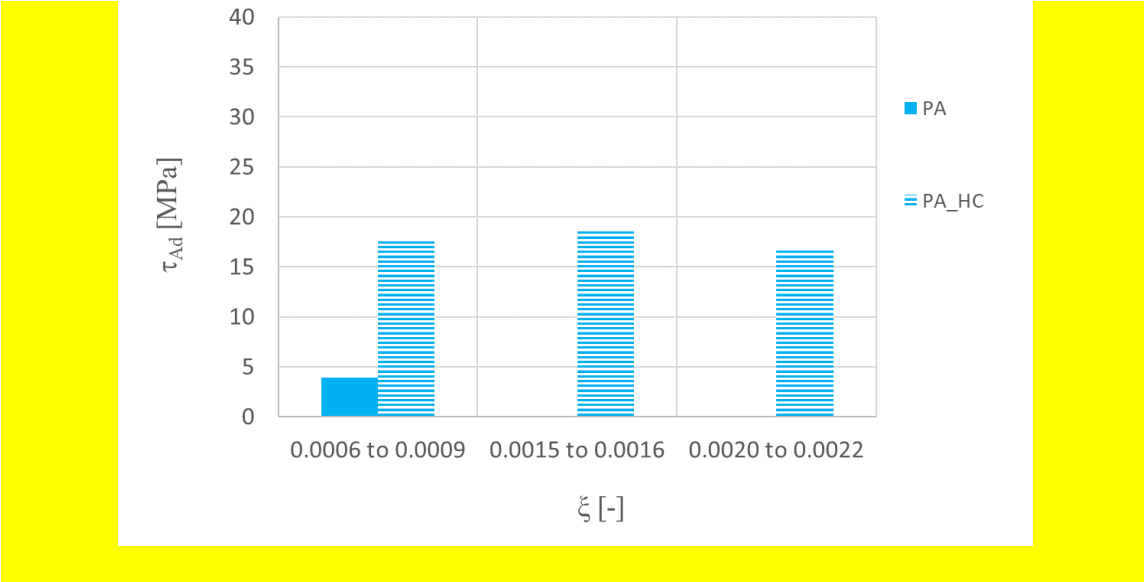

Figure 9: Adhesive shear strength (average values) for press-fitted specimens: smooth geometry (PA) vs. hoop-channeled one (PA_HC)

The advantages introduced by the hoop channel geometry are not found in the case of shrink-fit couplings (Fig. 10). The results indicate the joint resistance is even decreased by the new geometry. The same statistical tools indicate the decoupling force drop is not significant for the highest interference level, whereas it turns to be relevant for the medium and low ones. This occurrence may be explained, considering that a higher interference contribution is normally present under shrink-fitting, as roughness crests are not flattened. Moreover, upon coupling, a much higher amount of adhesive is retained as an effect of hub expansion. Consequently, when hoop channels are present, the aforementioned effect concerning the decrease of the nominal mating area for friction prevails on the other beneficial ones. It is worth mentioning the decoupling force is always lower than that retrieved for smooth shafts. From the quantitative point of view, it can be observed that at the two top levels of interference, on one hand the friction-related force is decreased by 15%, corresponding to the same decrease of the available mating area in

the channeled geometry. On the other hand, the adhesive contribution keeps barely unchanged regardless of hoop channels presence. Therefore, the overall decoupling force experiences an overall significant decrease, when comparing SA to SA_HC sample responses.

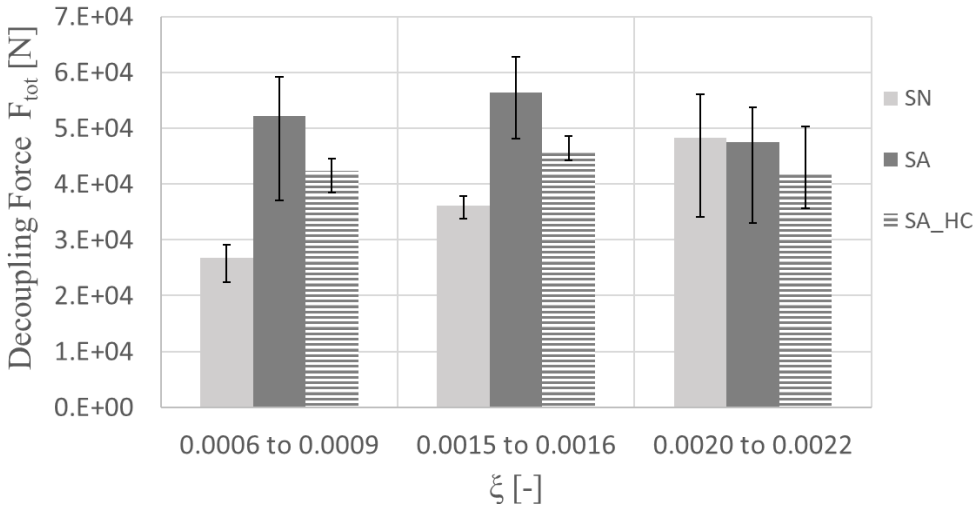

Figure 10: Decoupling force for shrink-fitted specimens. SN: dry coupled with smooth geometry; SA: coupled with adhesive with smooth geometry; SA_HC: coupled with adhesive with hoop channels

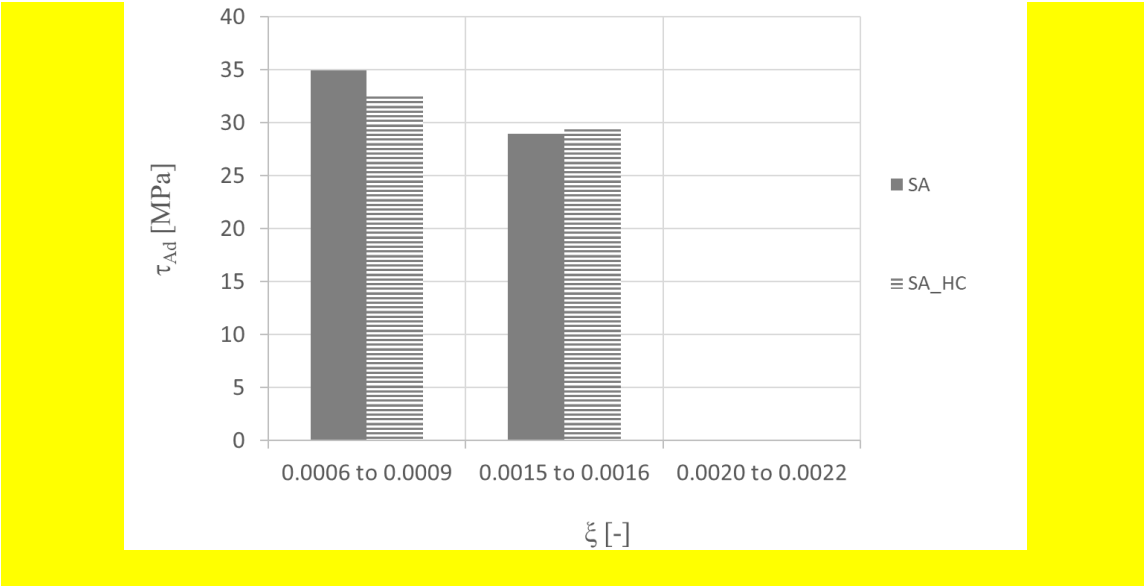

Figure 11: Adhesive shear strength (average values) for shrink-fitted specimens: smooth geometry (SA) vs. hoop-channeled one (SA_HC)

The same analysis has been run, to work out the adhesive shear strength for shrink-fitted couplings. The results displayed in Fig. 11 indicate the adhesive works properly at low

and medium specific interference levels: in this case, the retrieved strengths are independent of geometry (smooth vs channeled geometry) and well aligned with the typical properties of the adhesive. Smooth geometry is in this case sufficient to retain the adhesive, thanks to hub heating, and, therefore, hoop channels do not add any beneficial contribution. This is a further proof it is the reduction of the interference-related term to be responsible for overall joint resistance worsening. At the highest interference level, hoop channels yield a generally negligible contribution to adhesive response enhancement.

5. Conclusions

This study has been focused on the behavior of a shaft-hub hybrid joints and was motivated by the lack of studies dealing with temperature effect on anaerobic adhesives under high interference and with possible approaches to overcome the issue of adhesive being stripped away upon coupling, especially under press-fitting. Push-out tests involving shafts made of 42CrMo4 tempered steel and hubs made of 16CrNi4Pb hardening steel bonded by LOCTITE 648 were performed. In the first part, the influence of temperature on the joint static resistance and on the adhesive strength was investigated, accounting also for other design-related factors, namely the assembly process and the interference level. Specimens were coupled by press-fitting and shrink-fitting at four interference levels (up to 0.2%), and they were decoupled at 100°C. Results highlight that the decoupling force decreases as temperature increases. If compared to room temperature tests, a release force reduction by 26% in press-fitted samples and by 28% in shrink-fitted ones was observed. The adhesive shear strength was also estimated and its degradation was correlated to the glass transition temperature threshold and to the interference level. It was observed that high temperature is critical in hybrid joints, as it detrimentally affects not only the adhesive strength, but also the friction coefficient, which decreases as

temperature rises. The combined effect leads to an axial release force that is even lower than that achievable without adhesive at room temperature. Temperature response investigation was limited to the level of 100°C that is a realistic level for a gearbox and also corresponds to the adhesive glass transition temperature. It seemed to be reasonable not to consider higher temperature levels, as they would have been unfeasible for the considered application. However, this could be the topic of a further investigation.

Based on the occurrence that adhesive becomes ineffective for a specific interference beyond 0.0011 for press-fitted samples, as it is completely teared off upon coupling, a possible strategy was investigated to overcome this issue. In the second part of the study specimens, where the shafts are properly machined with hoop channels were considered for this purpose. Press-fitted and shrink-fitted joints with different specific interference (up to 0.2%) were considered. Decoupling tests were run and statistical tools (analysis of variance, orthogonality and pairwise tests) were applied to isolate the effects of hoop channels.

The results indicate that, for press-fitted joints, even at high interference, the hoop channels act as adhesive reservoir and facilitate adhesive dragging over the entire coupling length. Furthermore, the hoop channel areas operate as a pin-and-collar joint. The determined shear strength of the adhesive ensures that it is a correctly retained at the interface, thus efficiently contributing to the joint performance. This beneficial effect is highly significant and prevails on the reduction of the available mating area for interference fitting. Conversely, for shrink-fitted joints, for which the occurrence of adhesive stripping is more reduced, cutting hoop channels does not enhance the adhesive performance. In addition, it entails a lower engagement length for interference, which implies a significant reduction of the interference-related contribution, and, in turn, of the joint overall resistance, with respect to smooth geometry.

References

[1] Williams, D. Adhesives in the assembly of automotive drive-line equipment. *Int. J. Adhes. Adhes.* **1984**, *4*, 9-12. DOI:10.1016/0143-7496(84)90054-X.

[2] Ocaña, R.; Arenas, J. M.; Alía, C.; Narbón, J. J. Evaluation of degradation of structural adhesive joints in functional automotive applications. *Procedia Eng.* **2015**, *132*, 716-723. DOI:10.1016/j.proeng.2015.12.552.

[3] Deb, A.; Malvade, I.; Biswas, P.; Schroeder, J. An experimental and analytical study of the mechanical behaviour of adhesively bonded joints for variable extension rates and temperatures. *Int. J. Adhes. Adhes.* **2008**, *28*, 1-15. DOI:10.1016/j.ijadhadh.2007.02.004.

[4] Croccolo, D.; De Agostinis, M.; Vincenzi, N. Design and optimization of shaft-hub Hybrid joints for lightweight structures: analytical definition of normalizing parameters. *Int. J. Mech. Sci.* **2012**, *56*, 77-85.

[5] Croccolo, D.; De Agostinis, M.; Vincenzi, N. Design of hybrid steel-composite interference fitted and adhesively bonded connections. *Int. J. Adhes. Adhes.* **2012**, *37*, 19-25.

[6] Périchaud, M. G.; Delétage, J. Y.; Frémont, H.; Danto, Y.; Faure, C. Reliability evaluation of adhesive bonded SMT components in industrial applications. *Microelectron. Reliab.* **2000**, *40*, 1227-1234.

[7] Gilleo, K. Assembly with conductive adhesives. *Solder. Surf. Mt. Technol.* **1995**, *19*, 12-17.

[8] White, K. L.; Sue, H. Electrical conductivity and fracture behavior of epoxy/polyamide-12/ multiwalled carbon nanotube composites. *Polym. Eng. Sci.* **2011**, *51*, 2245-2253. DOI:10.1002/pen.21996.

[9] Warren, G. L.; Sun, L.; Hadjiev, V. G.; Davis, D.; Lagoudas, D.; Sue, H. B-staged epoxy/single-walled carbon nanotube nanocomposite thin films for composite reinforcement. *J. Appl. Polym. Sci.* **2009**, *112*, 290-298. DOI:10.1002/app.29375.

[10] Da Silva, L. F. M.; Adams, R. D. Joint Strength Predictions for Adhesive Joints to Be Used over a Wide Temperature Range. *Int. J. Adhes. Adhes.* **2007**, *27*, 362-379. DOI:10.1016/j.ijadhadh.2006.09.007.

[11] Da Silva, L. F. M.; Adams, R. D. Adhesive Joints at High and Low Temperatures Using Similar and Dissimilar Adherends and Dual Adhesives. *Int. J. Adhes. Adhes.* **2007**, *27*, 216-226. DOI:10.1016/j.ijadhadh.2006.04.002.

[12] Da Silva, L. F. M.; Adams, R. D.; Gibbs, M. Manufacture of Adhesive Joints and Bulk Specimens with High-temperature Adhesives. *Int. J. Adhes. Adhes.* **2004**, *24*, 69-83. DOI:10.1016/S0143-7496(03)00101-5.

[13] Da Silva, L. F. M.; Adams, R. D. Stress-free temperature in a mixed-adhesive joint. *J. Adhes. Sci. Technol.* **2006**, *20*, 1705-1726. DOI:10.1163/156856106779024436.

[14] Croccolo, D.; De Agostinis, M.; Fini, S.; Olmi, G. Influence of the engagement ratio on the shear strength of an epoxy adhesive by push-out tests on pin-and-collar joints: Part II: Campaign at different temperature levels. *Int. J. Adhes. Adhes.* **2016**, *67*, 76-85. DOI:10.1016/j.ijadhadh.2015.12.029.

[15] Petrova, A. P.; Kulikov, V. V.. Properties of adhesive materials used in repair-and-renewal operations. *Polym. Sci. - D* **2009**, *2*, 34-43. DOI:10.1134/S1995421209010079.

[16] Osterndorf, J. F.; Bonk, R. B. Evaluating adhesives for aluminum-to-copper bonding. *Adhes. Age* **1991**, *34*, 24-27.

[17] Karnolt, C. L. Anaerobic adhesives for sheet metal assembly, Proceedings of the SAE Automotive Engineering Congress and Exposition, Detroit, MI, February 24-28, 1975; SAE Paper No. 750140.

[18] Mengel, R.; Häberle, J.; Schlimmer, M. Mechanical properties of hub/shaft joints adhesively bonded and cured under hydrostatic pressure. *Int. J. Adhes. Adhes.* **2007**, *27*, 568-573. DOI:10.1016/j.ijadhadh.2006.11.003.

[19] Wojtczak, E.; Rucka, M. Monitoring the curing process of epoxy adhesive using ultrasound and lamb wave dispersion curves. *Mech Syst Signal Process.* **2021**, *151*, DOI:10.1016/j.ymssp.2020.107397.

[20] Croccolo, D.; De Agostinis, M.; Fini, S.; Olmi, G.; Paiardini, L.; Robusto, F. Influence of the interference level and of the assembly process on the shear strength of loctite 648 anaerobic adhesive. *J. Adhes.* **2020**, *96*, 90-112. DOI:10.1080/00218464.2019.1681268.

[21] Castagnetti, D.; Dragoni, E. Experimental Assessment of a Micro-Mechanical Model for the Static Strength of Hybrid Friction-Bonded Interfaces. *J. Adhes.* **2013**, *89*, 642-659. DOI: 10.1080/00218464.2012.747179.

[22] Sekercioglu, T.; Gulsoz, A.; Rende, H.; Meran, C. The Effects of Surface Roughness on the Strength of Adhesively Bonded Cylindrical Components. *J. Mater. Process. Technol.* **2003**, *142*, 82-86. DOI: 10.1016/S0924-0136(03)00463-1.

[23] Rudawska, A.; Danczak, I.; Müller, M.; Valasek, P. The effect of sandblasting on surface properties for adhesion. *Int. J. Adhes. Adhes.* **2016**, *70*, 176-190. DOI:10.1016/j.ijadhadh.2016.06.010.

[24] Harris, A. F.; Beevers, A. Effects of grit-blasting on surface properties for adhesion. *Int. J. Adhes. Adhes.* **1999**, *19*, 445-452. DOI:10.1016/S0143-7496(98)00061-X.

[25] Wu, Y.; Lin, J; Carlson, B. E.; Lu, P; Balogh, M. P.; Irish, N. P.; Mei, Y. Effect of laser ablation surface treatment on performance of adhesive-bonded aluminum alloys. *Surf. Coat. Technol.*, **2016**, *304*, 340-347.

[26] Broad, R.; French, J.; Sauer J. New, effective, ecological surface pretreatment for highly durable adhesively bonded metal joints. *Int. J. Adhes. Adhes.*, **1999**, *19*, 193-198.

[27] Critchlow, G. W.; Brewis, D. M.; Emmony, D. C.; Cottam, C. A. Initial investigation into the effectiveness of CO_2-laser treatment of aluminium for adhesive bonding. *Int. J. Adhes. Adhes.*, **1995**, *15*, 233-236.

[28] Spaggiari, A.; Dragoni, E. Effect of Mechanical Surface Treatment on the Static Strength of Adhesive Lap Joints. *J. Adhes.*, **2013**, *89*, 677-696.

[29] Borsellino, C.; Di Bella, G.; Ruisi V. F. Effect of chemical etching on adhesively bonded Aluminum AA6082. *Key Eng. Mater.*, **2007**, *344*, 669-676.

[30] Dragoni, E.; Mauri, P. Intrinsic static strength of friction interfaces augmented with anaerobic adhesives. *Int. J. Adhes. Adhes.*, **2000**, *20*, 315-321.

[31] Dragoni, E.; Mauri, P. Cumulative static strength of tightened joints bonded with anaerobic adhesives. *Proc. Inst. Mech. Eng. L*, **2002**, *216*, 9-15.

[32] Carbas, R. J. C.; Marques, E. A. S.; Da Silva, L. F. M.; Lopes, A. M.. Effect of cure temperature on the glass transition temperature and mechanical properties of epoxy adhesives. *J. Adhes.* **2014**, *90*, 104-119. DOI:10.1080/00218464.2013.779559.

[33] Pearson, S. R.; Shipway, P. H.; Abere, J. O.; Hewitt, R. A. A. The effect of temperature on wear and friction of a high strength steel in fretting. *Wear* **2013**, *303*, 622-631. DOI:10.1016/j.wear.2013.03.048.

[34] Kayaba, T.; Iwabuchi, A. The fretting wear of 0.45% C steel and austenitic stainless steel from 20 to 650 °C in air. *Wear* **1981**, *74*, 229-245. DOI:10.1016/0043-1648(81)90165-4.